

Antiprotons from dark matter annihilation through light mediators and a possible excess in AMS-02 \bar{p}/p data

Xian-Jun Huang, Chun-Cheng Wei, Yue-Liang Wu, Wei-Hong Zhang, and Yu-Feng Zhou

*CAS Key Laboratory of Theoretical Physics, Institute of Theoretical Physics,
Chinese Academy of Sciences, ZhongGuanCun East Road 55, Beijing 100190, China
and University of Chinese Academy of Sciences, Yuquan Road 19A, Beijing 100049, China*
(Received 15 November 2016; published 31 March 2017)

We show that in the scenario where dark matter (DM) particles annihilate through light mediators, the energy spectra of the final state cosmic-ray particles depend strongly on the mediator mass. For final state antiprotons, a spectrum with relatively narrow peak occurs when the mediator mass is comparable to the $\bar{p}p$ production threshold. Of interest, the latest AMS-02 data on the \bar{p}/p flux ratio hint at a bumplike excess over the expected background in the energy range $\sim 100\text{--}450$ GeV. We show that such a light mediator scenario is favored by the latest AMS-02 data over the scenarios of DM direct annihilation into the standard model particles and that of antiprotons produced from inside supernova remnants (SNRs), and is consistent with the upper limits derived from the Fermi-LAT data on the gamma rays towards the dwarf spheroidal galaxies. The \bar{p}/p flux ratio with energy above 450 GeV is predicted to fall with energy quickly, which can be easily distinguished from the other two scenarios as they predict the ratio to be flattening or rising up to the multi-TeV region.

DOI: [10.1103/PhysRevD.95.063021](https://doi.org/10.1103/PhysRevD.95.063021)

I. INTRODUCTION

Cosmic-ray (CR) antiparticles such as positrons and antiprotons are relatively rare and sensitive to exotic contributions. In recent years, an excess over the expected background in CR positrons has been observed [1]. The spectral feature of the excess plays an important role in identifying its origin such as nearby astrophysical sources or dark matter (DM) interactions. Recently, the AMS-02 Collaboration published the measurement on the antiproton to proton (\bar{p}/p) flux ratio up to kinetic energy 450 GeV, based on four years of data taking [2], confirming the first preliminary result presented in the year 2015 [3]. Although the measured kinetic energy spectrum of the \bar{p}/p ratio is in overall agreement with the secondary production, especially below ~ 100 GeV [4,5], at higher energies, there is a trend of flattening and smooth rise in the range $\sim 100\text{--}260$ GeV, followed by a drop by $\sim 30\%$ in the range $\sim 260\text{--}450$ GeV. Such a hint of a bumplike excess has already been observed in the preliminary AMS-02 result [3], and is strengthened in the latest data with higher statistics.

This intriguing possibility of an excess with a distinctive spectral feature in the \bar{p}/p flux ratio, if confirmed, may shed light on the nature of its origin: (i) The pulsar wind nebulae are unlikely to produce energetic antiprotons. (ii) In the leading astrophysical explanation, extra antiprotons can be produced from collisions of primary CRs with the gas inside supernova remnants (SNRs); the resulting energy spectrum, however, features a continued flattening or weak rise at least up to 1 TeV for a typical cutoff energy $\mathcal{E}_{\text{max}} \sim \mathcal{O}(10)$ TeV [6,7]. (iii) The spectrum of antiprotons produced from halo DM annihilation directly into standard model (SM) final states in general features a very broad bump due to the long

chain of cascade showers and hadronization of the final state partons. Since there is little room left for extra contributions below ~ 100 GeV, the DM particle mass m_χ is pushed to be very high ($m_\chi \gtrsim 2$ TeV) [4,5,8,9]. Consequently, only the spectral tail of DM produced antiprotons can extend to the energy range accessible to the current AMS-02 experiment ($E \lesssim 450$ GeV); thus again a flattening or weak rise of the \bar{p}/p ratio is expected in this region.

In this paper, we show that in a class of scenarios where DM particles annihilate through light color-singlet mediators, the energy spectrum of a final state particle can be a narrow bump with reduced multiplicity. For antiprotons, a narrow peak occurs when the mediator mass is comparable to the $\bar{p}p$ production threshold $2m_p$. We show that such a light mediator scenario is favored by the latest AMS-02 data over the scenario of DM direct annihilation and that of antiprotons produced from inside of SNRs, and is also consistent with the known constraints such as the gamma-ray limits from the dwarf spheroidal galaxies (dSphs). The \bar{p}/p ratio in the high-energy range is predicted to fall with energy quickly, which makes it highly distinguishable from the other two scenarios.

II. EFFECTS OF MEDIATORS

The annihilation of DM particles provides an extra primary source of CR particles. The corresponding primary source term for a final state particle f takes the form

$$q(\mathbf{r}, E) = \frac{\rho(\mathbf{r})^2}{2m_\chi^2} \langle \sigma v \rangle \frac{dN}{dE}, \quad (1)$$

where $\langle \sigma v \rangle$ is the velocity-averaged DM annihilation cross section multiplied by DM relative velocity, $\rho(\mathbf{r})$ is the DM energy density distribution function, and dN/dE is the

spectrum of kinetic energy E which is related to the total energy \mathcal{E} as $E = \mathcal{E} - m_f$ with m_f the mass of the final state particle f .

In many well-motivated DM models, the DM particles do not couple to the SM particles directly, but through some light color-singlet mediator particles, which has rich phenomenological consequences in DM annihilation [10–12], self-scatterings [13–15] and solar capture [16,17], and direct detections [18,19]. In this scenario, for the same DM mass, the resulting energy spectrum of a final state particle from DM annihilation can be significantly different from the case without a mediator. Let us consider DM annihilating first into two mediators $\bar{\chi}\chi \rightarrow 2\varphi$ and followed by the decay $\varphi \rightarrow f + X$, where X stands for any other final states. The spectrum $dN(x)/dx$ of the scaled total energy $x = \mathcal{E}/m_\chi$ in the DM center-of-mass frame is related to that in the mediator rest frame $dN(x')/dx'$ (with $x' = 2\mathcal{E}'/m_\varphi$) by a Lorentz boost

$$\frac{dN(x)}{dx} = 2 \int_{a(x)}^{b(x)} dx' \frac{1}{\sqrt{1 - \varepsilon_1^2} \sqrt{x'^2 - \varepsilon_0^2}} \frac{dN(x')}{dx'}, \quad (2)$$

where the two parameters $\varepsilon_1 = m_\varphi/m_\chi$ and $\varepsilon_0 = 2m_f/m_\varphi$ characterize the mass hierarchies in the two-step cascade process. The lower and upper limits of the integration are $a(x) = x_-$ and $b(x) = \min\{1, x_+\}$ with $x_\pm = 2(x \pm \sqrt{(1 - \varepsilon_1^2)(x^2 - \varepsilon_1^2 \varepsilon_0^2/4)})/\varepsilon_1^2$. In the large hierarchy limit $\varepsilon_0 \ll 1$, Eq. (2) reproduces the known result in Refs. [20,21].

In general, Lorentz boosts at random directions tend to broaden the energy spectrum. However, the effect of broadening can be kinematically suppressed. In the simplest case where f is monoenergetic with energy $\bar{\mathcal{E}}'$, i.e. $dN/\mathcal{E}' \propto \delta(\bar{\mathcal{E}}' - \mathcal{E}')$ in the mediator rest frame, the spectrum boosted to the DM center-of-mass frame is a box-shaped spectrum with a center energy $\bar{\mathcal{E}}$ and width $\Delta\mathcal{E}$,

$$\bar{\mathcal{E}} = \gamma_B \bar{\mathcal{E}}', \quad \Delta\mathcal{E}/\bar{\mathcal{E}} = 2\beta_B \beta', \quad (3)$$

where $\gamma_B = 1/\varepsilon_1$ is the Lorentz boost factor, $\beta_B = (1 - \varepsilon_1^2)^{1/2}$ is the boost velocity, and $\beta' = (1 - m_f^2/\bar{\mathcal{E}}'^2)^{1/2}$ is the velocity of f in the mediator rest frame. In the case where f is a photon, $\beta' = 1$, a narrow-box spectrum can appear only when $\beta_B \ll 1$; namely, the mass of the mediator is close to that of the DM particle, $m_\varphi \approx m_\chi$, which can mimic a gamma-ray line (see e.g. [22]). In this work we consider the opposite case where $\beta' \ll 1$ and $\beta_B \approx 1$, corresponding to $m_\varphi \ll m_\chi$. For the decay of the mediator into light quarks $\varphi \rightarrow \bar{q}q \rightarrow \bar{p} + X$ ($q = u, d$), the velocity of the antiproton has an upper limit $\beta' \leq (1 - \varepsilon_0^2)^{1/2}$ as X at least contains a proton. Thus when $\varepsilon_0 \approx \mathcal{O}(1)$, namely, m_φ is comparable to the $\bar{p}p$ production threshold $2m_p$, the value of β' has to be small and the resulting spectrum is a narrow box in the DM halo rest frame. Furthermore, the total energy has a lower

limit $\bar{\mathcal{E}}' \geq m_p$, the value of $\bar{\mathcal{E}}$ can be very large for a large Lorentz boost factor $\gamma_B \gg 1$. Thus after the boost, the energy spectrum is a narrow box at high energy. Since the antiproton energy spectrum from the decay $\varphi \rightarrow \bar{q}q \rightarrow \bar{p} + X$ is low-energy dominated, the Lorentz boost will push the antiprotons into the high-energy region without significantly broadening the spectrum. On the contrary, the antiproton spectrum from DM direct annihilation $\chi\chi \rightarrow \bar{q}q$ is very broad for the same DM mass, due to the larger center-of-mass energy of the $\bar{q}q$ system and thus the longer chain of cascade parton showers and hadronization. Furthermore, in the light mediator scenario, the multiplicities of the final state particles are suppressed by the smallness of the mediator mass and can be much lower than that in the case without mediators. For the hadronic decay $\varphi \rightarrow \bar{q}q$, the energy spectrum dN/dx' of antiprotons is simulated using the Monte Carlo event generator Pythia 8.2 [23]. The \bar{p} multiplicity is found to be $N_p = 0.35, 1.2, 1.6$ and 3.0 for the center-of-mass energy $\mathcal{E}_{\text{CM}} = 10, 50, 100$ and 500 GeV, respectively. Thus for the same DM mass, the DM annihilation through light mediators will generate fewer antiprotons due to lower center-of-mass energy.

In Fig. 1, we show the spectra of the antiproton kinetic energy and photon energy from the annihilation $\chi\chi \rightarrow 2\varphi \rightarrow 2(\bar{q}q)$ of a 500 GeV DM particle with three different mediator masses, $m_\varphi = 5, 10$ and 50 GeV, respectively. For a

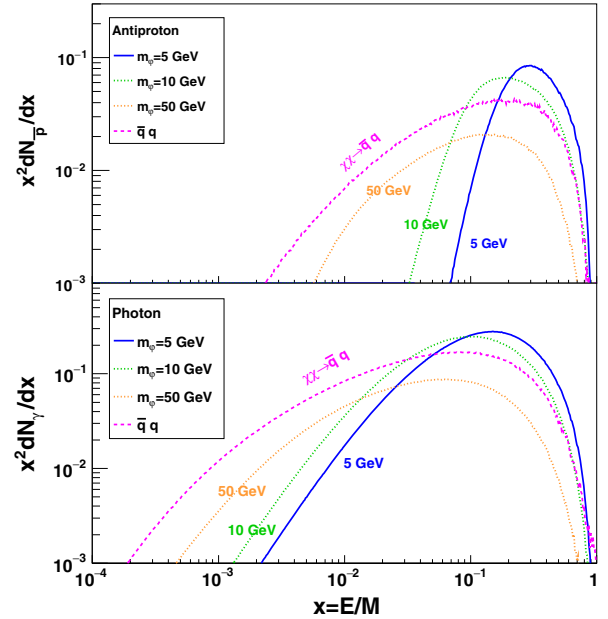


FIG. 1. Upper panel: Scaled energy spectra $x^2 dN/dx$ of antiprotons per DM annihilation from the annihilation $\chi\chi \rightarrow 2\varphi \rightarrow 2\bar{q}q$ ($q = u, d$) with mediator masses $m_\varphi = 5, 10$ and 50 GeV, respectively. The DM particle mass is fixed at $m_\chi = 500$ GeV. The spectrum of DM direct annihilation $\chi\chi \rightarrow \bar{q}q$ with the same DM mass is also shown. Lower panel: The same as the upper panel, but for photons.

comparison, the spectrum for DM direct annihilation $\chi\chi \rightarrow \bar{q}q$ for the same DM mass is also shown. For a very light mediator $m_\phi = 5$ GeV, the antiproton spectrum appears to be a narrow bump. As the mediator mass increases, the spectrum becomes broader. For $m_\phi = 50$ GeV, the spectrum looks similar to that from DM direct annihilation, but with lower multiplicity. Similar observations hold for the photon energy spectrum. The figure illustrates that the energy spectra of antiprotons and photons from DM annihilation can be highly model dependent, which will drastically change the interpretations of the experimental data. While the predictions from Pythia for low-energy hadronic processes have not been fully validated [24], the presence of the narrow-bump spectrum is a generic kinematical effect, and is insensitive to the details of the hadronization model.

III. SNR CONTRIBUTIONS

It has been suggested that extra secondary antiprotons can be generated from the collisions of primary CRs onto the gas inside the SNRs, and accelerated by the shock wave in the same way as that of the primary CRs [6,25–27]. This mechanism does not require new class of sources and predicts strong correlations between the spectra of secondary species such as positrons, antiprotons and heavy nuclei. We consider the setup in the rest frame of the shock front (at $x = 0$) where $u_1(u_2)$ and $n_1(n_2)$ are the upstream (downstream) plasma speed and density respectively. The compression factor $r = u_1/u_2 = n_2/n_1$ determines the power law index $\gamma = 3r/(r - 1)$ of the primary proton spectrum. The secondary antiprotons are produced inside SNRs and propagate in the same ways as primary protons, which largely cancels the effect of propagation. The \bar{p}/p flux ratio from solving the transportation equation for \bar{p} inside SNRs is given by [6]

$$\left(\frac{\Phi_{\bar{p}}}{\Phi_p}\right)_{\text{SNR}} \sim 2n_1 c \left[\gamma \left(\frac{1}{\xi} + r^2 \right) \int_{m_p}^{\mathcal{E}} d\omega \omega^{\gamma-3} \frac{D_1(\omega)}{u_1^2} I(\omega) + \frac{\tau_{\text{SNR}} r}{2\mathcal{E}^{2-\gamma}} I(\mathcal{E}) \right], \quad (4)$$

where the first (second) term in the square brackets corresponds to the generation of \bar{p} with (without) acceleration. The source function I is defined as $I(\omega) = \int_{\omega}^{\mathcal{E}_{\text{max}}} d\mathcal{E} \mathcal{E}^{2-\gamma} \sigma(\mathcal{E}, \omega)$, where $\sigma(\mathcal{E}, \omega)$ is the \bar{p} production cross section for the process $p(\mathcal{E}) + \text{H} \rightarrow \bar{p}(\omega) + X$, which is taken from [28]. The parameter ξ is the fraction of proton energy carried away by a secondary antiproton, and τ_{SNR} is the typical SNR age. The diffusion coefficient upstream is $D_1(\mathcal{E}) \approx 3.3 \times 10^{22} \mathcal{F}^{-1} (\mathcal{E}/\text{GeV}) (B/\mu\text{G})^{-1} \text{cm}^2 \text{s}^{-1}$. In the numerical calculation, we fix the parameters as $u_1 = 0.5 \times 10^8 \text{cm} \times \text{s}^{-1}$, $n_1 = 2 \text{cm}^{-3}$, $r = 3.8$, $\xi = 0.17$, and $\tau_{\text{SNR}} = 2 \times 10^4 \text{yr}$. For the parameters in the diffusion coefficients, we fix them as $\mathcal{F} = 1/20$ and $B = 1 \mu\text{G}$. Note that the normalization of the \bar{p}/p ratio is proportional

to the combination $N_{\text{SNR}} = n_1 u_1^{-2} B_{\mu\text{G}}^{-1} \mathcal{F}^{-1}$. There are some uncertainties in the cutoff energy \mathcal{E}_{max} which depends on the typical SNR age, but the typical value is $\mathcal{E}_{\text{max}} \approx \mathcal{O}(10\text{--}100) \text{TeV}$ [6,7]. From Eq. (4), one can see that the \bar{p}/p flux ratio increases monotonously with increasing energy \mathcal{E} and saturates when $\mathcal{E} \approx \mathcal{E}_{\text{max}}$. Thus the generic prediction of the model is a flattening and eventually a rise of the \bar{p}/p ratio in the 100 GeV to multi-TeV region.

The smoothly rising spectrum in the energy range 100–500 GeV is a common feature of the mechanisms with extra secondary \bar{p} generation from the collisions between the primary CRs and the gas either inside the SNRs [6,25–27] or in the dense clouds surrounding the SNRs [29,30]. This is due to the high scale of the typical maximum acceleration energy $E_{\text{max}} \sim \mathcal{O}(10) \text{TeV}$ and the power-law nature of the injection primary CRs. In models with inhomogeneous spatial diffusion such as the two-halo models [31–33], the power index δ of the diffusion coefficient is allowed to take different values in different halo regions, which can predict an enhancement of \bar{p}/p after adjusting the parameters to reproduce the hardening of the primary CRs [33]. The resulting \bar{p}/p spectrum is typically a combination of power-law spectra with different power indices. Thus again only a smooth rise can be obtained. The bumplike spectral feature with a significant drop at energy below $\sim 500 \text{GeV}$, if confirmed, will disfavor these astrophysical mechanisms.

IV. FIT TO AMS DATA

We compare the above-mentioned three scenarios of antiproton production: (A) DM annihilation into quarks through light mediators, (B) DM direct annihilation into quarks, and (C) antiprotons produced from the inside of SNRs through fitting to the high-energy AMS-02 antiproton data. We examine whether they are favored and can be distinguished by the current and future experiments. The propagation of the CR antiprotons is calculated using GALPROP v54 [34]. We consider three representative propagation models selected from a global Bayesian analysis to the AMS-02 proton and B/C data using the GALPROP code [35]. They are selected to represent the typically minimal (MIN), median (MED) and maximal (MAX) antiproton fluxes at 95% C.L. Note that these propagation models are different from and complementary to that given in Ref. [36] which are based on semianalytical solutions with simplified assumptions. The Einasto DM profile is adopted as a benchmark profile with a local DM density of $\rho_0 = 0.43 \text{GeV cm}^{-3}$. The effect of solar modulation is taken into account using the force-field approximation [37]. We use charge asymmetric Fisk potentials $\phi_p = 550 \text{MV}$ and $\phi_{\bar{p}}/\phi_p = 0.2$ which leads to a good agreement with the low-energy antiproton data [38].

We determine the model parameters through fitting to the AMS-02 data. Since we are only interested in the

high-energy part of the \bar{p}/p spectrum, only the \bar{p}/p data with $E \geq 20$ GeV (in total 26 data points) are included, which also largely avoids the uncertainties in modeling the solar modulation. Discussions on a possible \bar{p} excess at low energies can be found in Refs. [5,38,39]. The significance of an excess over the background is estimated using a test statistics $TS = -2 \ln(\mathcal{L}_{\text{bg}}/\mathcal{L}_{\text{bg+src}})$, where \mathcal{L}_{bg} and $\mathcal{L}_{\text{bg+src}}$ are the likelihood functions for the scenarios of background-only and background plus extra sources, respectively. In all the fits, the normalization of the secondary background is allowed to float freely, i.e. $\Phi_{\bar{p},\text{bg}} \rightarrow \kappa \Phi_{\bar{p},\text{bg}}$ with the normalization constant κ determined solely by data.

The fit to the data in the background-only scenario in the MED propagation model results in $\chi^2 = 22.8$ for 25 degrees of freedom (d.o.f.), suggesting a good agreement with the data. The best-fit background of the \bar{p}/p ratio is shown in Fig. 2. Despite the overall agreement, a hint of systematic deviation at energies above ~ 100 GeV can be seen clearly. The best-fit backgrounds in the MIN and MAX models are found to be very close to that in the MED model.

In scenario A, i.e., $\chi\chi \rightarrow 2q \rightarrow 2\bar{q}q$, we first consider the case of a 5 GeV mediator. The best-fit parameters, χ^2 and TS values are summarized in Tab. I. In the three propagation models, the favored DM masses are in the range 600 GeV—1 TeV. In the MED model, the best-fit cross section is compatible with the typical thermal cross section. From the MIN to the MAX model, the variation of the best-fit cross section is within an order of magnitude, which represents the typical uncertainties due to propagation

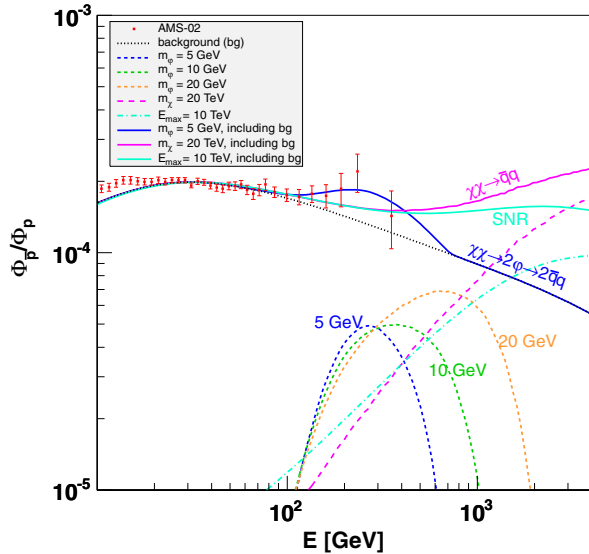


FIG. 2. Best-fit \bar{p}/p flux ratios from the three scenarios: scenario A with mediator mass $m_\phi = 5, 10$ and 20 GeV, respectively; scenario B with $m_\chi = 20$ TeV; and scenario C with $\mathcal{E}_{\text{max}} = 10$ TeV. The sum with the background in each scenario (for $m_\phi = 5$ GeV in scenario A) is also shown, together with the AMS-02 data [2].

models. Since the measured \bar{p}/p is very small and of $\mathcal{O}(10^{-4})$, it is a good approximation that the background and the new source contributions can be summed together in the \bar{p}/p flux ratio, i.e., $\Phi_{\bar{p}}/\Phi_p \approx (\Phi_{\bar{p},\text{bg}}/\Phi_p) + (\Phi_{\bar{p},\text{src}}/\Phi_p)$. In Fig. 2, the best-fit \bar{p}/p flux ratios together with the background in the MED model are shown. It can be seen that the structure in the AMS-02 data at ~ 300 GeV can be reproduced for $m_\phi = 5$ GeV. For heavier mediators, we find $m_\chi = 1.49(2.74)$ TeV, $\langle\sigma v\rangle = 9.4(23.2) \times 10^{-26} \text{ cm}^3 \text{ s}^{-1}$ and $\chi^2 = 14.3(14.9)$ for $m_\phi = 10(20)$ GeV, and the peaks of the best-fit spectra move to higher energies, which worsens the agreement with the data, and results in larger χ^2 values, as can be seen from Fig. 2.

In scenario B, i.e., $\chi\chi \rightarrow \bar{q}q$, we find that the current data impose a lower limit of $m_\chi \gtrsim 2$ TeV, confirming the previous analysis based on the preliminary data [5]. Introducing a heavier DM mass always improves the agreement with the data. However, after $m_\chi \gtrsim 10$ TeV, the value of χ^2 gradually ceases to decrease and approaches a constant. The reason is that for very heavy DM particles, only the low-energy tail of the DM generated antiproton spectrum can extend to the region accessible to the current AMS-02 experiment ($E \leq 450$ GeV). In this region, the increase of the DM mass leads to a lower \bar{p} flux which can be compensated by the increase of the annihilation cross section. In Tab. I, the fit results for fixed $m_\chi = 20$ TeV are shown. The corresponding best-fit \bar{p}/p ratio is shown in Fig. 2.

For scenario C, we use the expression of Eq. (4) plus a background contribution. Besides the normalization factor κ of the background, the normalization of the SNR contribution is also allowed to vary freely by introducing a factor η , i.e., $N_{\text{SNR}} \rightarrow \eta N_{\text{SNR}}$. The spectral shape of the SNR antiprotons is characterized by the maximal energy \mathcal{E}_{max} . Similar to the case of the DM direct annihilation,

TABLE I. Fit results for the three scenarios: scenario A with $m_\phi = 5.0$ GeV, scenario B with $m_\chi = 20$ TeV, and scenario C with $\mathcal{E}_{\text{max}} = 10$ TeV, in the MIN, MED and MAX propagation models. The cross section is in units of $10^{-26} \text{ cm}^3 \text{ s}^{-1}$. The numbers in the parentheses in scenario C stand for the values of the factor η .

	Model	m_χ (GeV)	$\langle\sigma v\rangle(\eta)$	κ	χ^2	TS
A	MIN	765_{-153}^{+167}	$18.6_{-8.0}^{+10.7}$	1.12 ± 0.01	12.5	11.6
	MED	808_{-165}^{+184}	$5.18_{-2.37}^{+3.04}$	1.13 ± 0.01	13.8	9.0
	MAX	826_{-168}^{+185}	$2.29_{-1.06}^{+1.31}$	1.13 ± 0.01	15.5	8.5
B	MIN	20000	1200 ± 410	1.12 ± 0.01	15.5	8.6
	MED	20000	291 ± 123	1.13 ± 0.01	17.2	5.6
	MAX	20000	117 ± 54	1.12 ± 0.01	19.3	4.7
C	MIN	...	(0.262 ± 0.103)	1.08 ± 0.02	17.6	6.5
	MED	...	(0.195 ± 0.104)	1.10 ± 0.02	19.2	3.5
	MAX	...	$(0.172_{-0.105}^{+0.104})$	1.10 ± 0.02	21.4	2.7

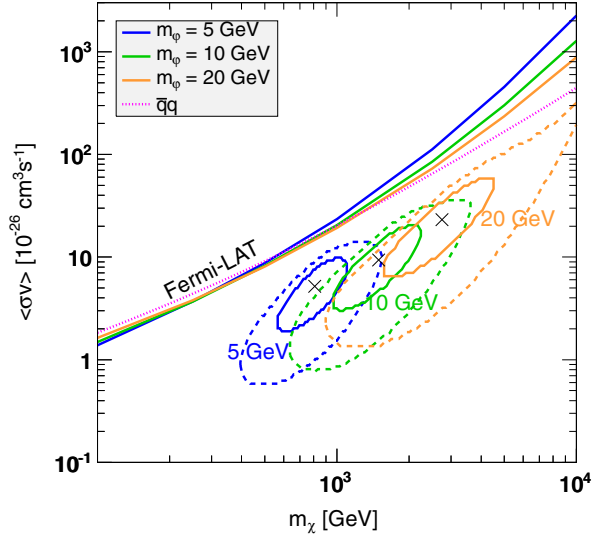


FIG. 3. Contours of favored regions by the AMS-02 data at 68% (solid) and 95% (dashed) C.L.'s in the $(m_\chi, \langle\sigma v\rangle)$ plane in scenario A with $m_\phi = 5, 10$ and 20 GeV, respectively. The crosses indicate the best-fit values. The 95% C.L. upper limits derived from the Fermi-LAT data on the dSphs are shown as the solid curves. The derived limits for scenario B are also shown.

we find that a SNR contribution with sufficiently large $\mathcal{E}_{\max} \sim \mathcal{O}(10)$ TeV can improve the agreement with the data, and the improvement gradually saturates when $\mathcal{E}_{\max} \gtrsim 10$ TeV, which is due to a similar degeneracy between \mathcal{E}_{\max} and the normalization factor η . We thus fix the cutoff \mathcal{E}_{\max} to be 10 TeV. The predicted spectrum of the \bar{p}/p ratio in the multi-TeV region is again a flattening and weak rise until the maximum energy \mathcal{E}_{\max} is reached.

The TS values of the three scenarios in the three propagation models are listed in Tab. I. It is clear that scenario A has the highest significance in all the propagation models. Due to the limited statistics, the current data cannot rule out scenarios B and C. There is a good opportunity that scenario A can be distinguished from B and C in the future, as the AMS-02 experiment will continue the data taking till 2024. In this scenario, as can be seen from Fig. 2, above 450 GeV, the \bar{p}/p ratio is expected to fall with energy, while in the other two scenarios, the spectra will continue to rise to higher energies. Thus this scenario can be distinguished easily from the other two by the future data at higher energies.

V. CONSTRAINTS

The most stringent and robust constraints so far on the DM annihilation cross sections arise from the observation of γ -rays towards dSphs by the Fermi-LAT Collaboration [40]. Due to the significant difference in the spectra shape, the reported Fermi-LAT limits do not apply to the case where DM annihilates through mediators. We derive the upper limits directly from the likelihood profile per energy bin of gamma rays provided by the Fermi-LAT Collaboration for a selection of 15 dSphs with high-confidence J-factors and backgrounds [41]. As a cross-check, in Fig. 3 we show the derived upper limits for the DM direct annihilation $\chi\chi \rightarrow \bar{q}q$ which well reproduces the result of Fermi-LAT [40]. The limits for the case with $m_\phi = 5, 10$ and 20 GeV are shown in Fig. 3, together with the regions allowed by the AMS-02 data. The favored regions are all consistent with the current limits. The derived upper limits turn out to be dependent on the mediator mass at a high DM mass region. Compared with the direct DM annihilation, we find that at high energies around 10 TeV, the derived upper limit is weaker by a factor of 5. This is due to the fact that for a multi-TeV DM particle, the relatively narrow γ -ray spectrum shown in Fig. 1 has a smaller fraction of photons entering into the low-energy region accessible to the Fermi-LAT experiment, which results in less stringent constraints.

In the scenario of DM annihilation into light quarks through mediators, we find that the predicted positron fraction is at most 4×10^{-4} for $m_\phi = 5$ GeV, which is far below the expected background $\sim \mathcal{O}(10^{-2})$ [35,42]. Thus the constraints from the positron fraction are rather weak. The current LHC search for mono-X plus missing energy can only impose constraints on the mediator mass in the case of $m_\phi > 2m_\chi$ [43], which makes it less relevant to the case of DM annihilation with light mediators.

ACKNOWLEDGMENTS

Y. L. W. is grateful to S. Ting for warm hospitality and discussions during his visit to the AMS-02 Collaboration at CERN. This work is supported by the National Science Foundation of China (NSFC) under Grants No. 11335012 and No. 11475237. This work is also partly supported by the Key Research Program of Frontier Sciences, CAS and Strategic Priority Research Program of CAS Grant No. XDB23030000.

- [1] O. Adriani *et al.*, *Astropart. Phys.* **34**, 1 (2010); M. Ackermann *et al.* (Fermi-LAT Collaboration), *Phys. Rev. Lett.* **108**, 011103 (2012); L. Accardo *et al.* (AMS Collaboration), *Phys. Rev. Lett.* **113**, 121101 (2014).
- [2] M. Aguilar *et al.* (AMS Collaboration), *Phys. Rev. Lett.* **117**, 091103 (2016).
- [3] S. Ting, AMS-02 days at CERN, Geneva.
- [4] G. Giesen, M. Boudaud, Y. Gnolini, V. Poulin, M. Cirelli, P. Salati, and P. D. Serpico, *J. Cosmol. Astropart. Phys.* **09** (2015) 023.
- [5] H.-B. Jin, Y.-L. Wu, and Y.-F. Zhou, *Phys. Rev. D* **92**, 055027 (2015).
- [6] P. Blasi and P. D. Serpico, *Phys. Rev. Lett.* **103**, 081103 (2009).
- [7] P. Mertsch and S. Sarkar, *Phys. Rev. D* **90**, 061301 (2014).
- [8] S.-J. Lin, X.-J. Bi, P.-F. Yin, and Z.-H. Yu, arXiv:1504.07230.
- [9] M. Ibe, S. Matsumoto, S. Shirai, and T. T. Yanagida, *Phys. Rev. D* **91**, 111701 (2015).
- [10] J. Hisano, S. Matsumoto, and M. M. Nojiri, *Phys. Rev. Lett.* **92**, 031303 (2004); N. Arkani-Hamed, D. P. Finkbeiner, T. R. Slatyer, and N. Weiner, *Phys. Rev. D* **79**, 015014 (2009); J. L. Feng, M. Kaplinghat, and H. B. Yu, *Phys. Rev. Lett.* **104**, 151301 (2010).
- [11] Z.-P. Liu, Y.-L. Wu, and Y.-F. Zhou, *Phys. Rev. D* **88**, 096008 (2013).
- [12] J. Chen and Y.-F. Zhou, *J. Cosmol. Astropart. Phys.* **04** (2013) 017.
- [13] A. Loeb and N. Weiner, *Phys. Rev. Lett.* **106**, 171302 (2011).
- [14] S. Tulin, H.-B. Yu, and K. M. Zurek, *Phys. Rev. Lett.* **110**, 111301 (2013).
- [15] M. Kaplinghat, T. Linden, and H.-B. Yu, *Phys. Rev. Lett.* **114**, 211303 (2015).
- [16] J. Chen, Z.-L. Liang, Y.-L. Wu, and Y.-F. Zhou, *J. Cosmol. Astropart. Phys.* **12** (2015) 021.
- [17] Z.-L. Liang, Y.-L. Wu, Z.-Q. Yang, and Y.-F. Zhou, *J. Cosmol. Astropart. Phys.* **09** (2016) 018.
- [18] T. Li, S. Miao, and Y.-F. Zhou, *J. Cosmol. Astropart. Phys.* **03** (2015) 032.
- [19] E. Del Nobile, M. Kaplinghat, and H.-B. Yu, *J. Cosmol. Astropart. Phys.* **10** (2015) 055.
- [20] J. Mardon, Y. Nomura, D. Stolarski, and J. Thaler, *J. Cosmol. Astropart. Phys.* **05** (2009) 016.
- [21] G. Elor, N. L. Rodd, and T. R. Slatyer, *Phys. Rev. D* **91**, 103531 (2015).
- [22] Y. Bai and J. Shelton, *J. High Energy Phys.* **12** (2012) 056.
- [23] T. Sjostrand, S. Mrenna, and P. Z. Skands, *Comput. Phys. Commun.* **178**, 852 (2008).
- [24] D. Muller (BABAR Collaboration), arXiv:1310.0520.
- [25] P. Mertsch and S. Sarkar, *Phys. Rev. Lett.* **103**, 081104 (2009).
- [26] E. G. Berezhko and L. T. Ksenofontov, *Astrophys. J.* **791**, L22 (2014).
- [27] M. Kachelrie, A. Neronov, and D. V. Semikoz, *Phys. Rev. Lett.* **115**, 181103 (2015).
- [28] L. C. Tan and L. K. Ng, *Phys. Rev. D* **26**, 1179 (1982).
- [29] Y. Fujita, K. Kohri, R. Yamazaki, and K. Ioka, *Phys. Rev. D* **80**, 063003 (2009).
- [30] K. Kohri, K. Ioka, Y. Fujita, and R. Yamazaki, *Prog. Theor. Exp. Phys.* **2016**, 021E01 (2016).
- [31] N. Tomassetti, *Astrophys. J.* **752**, L13 (2012).
- [32] Y.-Q. Guo, Z. Tian, and C. Jin, *Astrophys. J.* **819**, 54 (2016).
- [33] J. Feng, N. Tomassetti, and A. Oliva, *Phys. Rev. D* **94**, 123007 (2016).
- [34] A. W. Strong and I. V. Moskalenko, *Astrophys. J.* **509**, 212 (1998).
- [35] H.-B. Jin, Y.-L. Wu, and Y.-F. Zhou, *J. Cosmol. Astropart. Phys.* **09** (2015) 049.
- [36] F. Donato, N. Fornengo, D. Maurin, and P. Salati, *Phys. Rev. D* **69**, 063501 (2004).
- [37] L. J. Gleeson and W. I. Axford, *Astrophys. J.* **154**, 1011 (1968).
- [38] D. Hooper, T. Linden, and P. Mertsch, *J. Cosmol. Astropart. Phys.* **03** (2015) 021.
- [39] M.-Y. Cui, Q. Yuan, Y.-L. S. Tsai, and Y.-Z. Fan, arXiv:1610.03840.
- [40] M. Ackermann *et al.* (Fermi-LAT Collaboration), *Phys. Rev. Lett.* **115**, 231301 (2015).
- [41] L. M. Carpenter, R. Colburn, J. Goodman, and T. Linden, *Phys. Rev. D* **94**, 055027 (2016).
- [42] H.-B. Jin, Y.-L. Wu, and Y.-F. Zhou, *J. Cosmol. Astropart. Phys.* **11** (2013) 026.
- [43] M. Aaboud *et al.* (ATLAS Collaboration), *Phys. Rev. D* **94**, 032005 (2016); Report No. CMS-PAS-EXO-16-037.